Quantification of nanoscale density fluctuations using electron microscopy: Light-localization properties of biological cells

Prabhakar Pradhan,[1,a)] Dhwanil Damania,[1] Hrushikesh M. Joshi,[2] Vladimir Turzhitsky,[1] Hariharan Subramanian,[1] Hemant K. Roy,[3] Allen Taflove,[4] Vinayak P. Dravid,[2] and Vadim Backman[1]

[1]*Department of Biomedical Engineering, Northwestern University, Evanston, Illinois 60208, USA*
[2]*Department of Material Science and Engineering, Northwestern University, Evanston, Illinois 60208, USA*
[3]*Department of Internal Medicine, NorthShore University HealthSystem, Evanston, Illinois 60201, USA*
[4]*Department of Electrical Engineering and Computer Science, Northwestern University, Evanston, Illinois 60208, USA*

(Received 18 June 2010; accepted 9 November 2010; published online 17 December 2010)

We report a study of the nanoscale mass-density fluctuations of heterogeneous optical dielectric media, including nanomaterials and biological cells, by quantifying their nanoscale light-localization properties. Transmission electron microscope images of the media are used to construct corresponding effective disordered optical lattices. Light-localization properties are studied by the statistical analysis of the inverse participation ratio (IPR) of the localized eigenfunctions of these optical lattices at the nanoscale. We validated IPR analysis using nanomaterials as models of disordered systems fabricated from dielectric nanoparticles. As an example, we then applied such analysis to distinguish between cells with different degrees of aggressive malignancy. © *2010 American Institute of Physics*. [doi:10.1063/1.3524523]

Quantifying the degree of nanoscale disorder is a major research interest in characterizing the optical (electronic) properties of disordered condensed-matter systems.[1] Statistical properties, such as the mean and standard deviation (std), of the inverse participation ratio (IPR) of the spatially localized optical eigenfunctions of these optical systems are important quantitative measures of the degree of disorder of these lattices, where IPR of an eigenfunction E is defined as $\mathrm{IPR}=\int|E(r)|^4 d\vec{r}$ [in units of inverse area in two dimension (2D)].[2,3] The average value of the IPR of a uniform lattice is a fixed universal number (~2.5 in 2D), but the value increases with an increasing degree of disorder (or degree of localization). IPR has been well-studied in condensed-matter physics for characterizing the degree of disorder of homogeneous and heterogeneous media in a single parameter.[4–6]

In this paper, we report the study of light-localization properties of biological cells by first constructing optical lattices of these cells via transmission electron microscopy (TEM) imaging[7] and then studying the statistical properties of IPR of the eigenfunctions of these lattices. In our most recent optical experiments, we show that the degree of nanoscale disorder increases with the degree of carcinogenesis for both control and precancerous cells (in cell lines, mouse model, and different organs in human studies, such as pancreas, colon, and lung).[8–10] These nanoscale changes may result from the rearrangements of DNA, RNA, lipids, or proteins. We want to *verify* and *quantify* these nanoscale changes as observed in optical studies by TEM.

It has been shown that the optical refractive index (n) is linearly proportional to the local density (ρ) of intracellular macromolecules for a majority of the scattering substances found in living cells, such as proteins, lipids, DNA, or RNA, i.e., $n=n_0+\Delta n=n_0+\alpha\rho$, where n_0 is the refractive index of the medium, ρ is the local concentration of solids, with $\alpha \sim 0.18$.[11] Furthermore, we consider that the absorption of the contrast agent by the cell is linearly proportional to the total mass present in the thin cell voxel. Therefore, if TEM imaging is performed through a thin biological sample and we assume that (i) the TEM intensity $[I_{\mathrm{TEM}}(x,y)]$ is linearly proportional to the mass density of the voxel $[M(x,y)]$ and (ii) the refractive index of the voxel $[n(x,y)]$ is proportional to the mass density, then we can write $n(x,y)\propto M(x,y)\propto I_{\mathrm{TEM}}(x,y)$. Let $n(x,y)=n_0(x,y)+\Delta n(x,y)$.[12,13] Consequently, it can be shown that the effective (average) optical potential of an optical lattice, ε_i, for the voxel around the point (x,y) is

$$\varepsilon_i \propto \Delta n/n_0 = \Delta I_{\mathrm{TEM}}/I_{0\mathrm{TEM}}, \tag{1}$$

where $\Delta I_{\mathrm{TEM}}(x,y) \ll I_{0\mathrm{TEM}}(x,y)$; that is, $\Delta n(x,y) \ll n_0(x,y)$ (e.g., for tissue, $n_0=1.33-1.4$, and $\Delta n=0.01-0.1$).[1,14]

Tight-binding model. To quantify the disorder properties of the TEM images, we have carried out the Anderson disorder tight-binding model (TBM) calculation, which has proven to be a good model for describing single-optical states of systems of any geometry and disorder. Specifically, TBM Hamiltonian can be written as[1,14]

$$H=\sum_i \varepsilon_i|i\rangle\langle i| + t\sum_{\langle ij\rangle}|i\rangle\langle j| + |j\rangle\langle i|, \tag{2}$$

where $\varepsilon_i(x,y)\propto\Delta n(x,y)/n_0$ is the ith lattice site potential energy; $|i\rangle$ and $|j\rangle$ are the optical wave functions at the ith and jth lattice sites, respectively; $\langle ij\rangle$ indicates the nearest neighbors; and t is the overlap integral between the sites i and j. Now, entering the value of $\varepsilon_i(x,y)$ from Eq. (1) into Eq. (2), we can define the average IPR value over a pixel[4–6]

$$\langle \mathrm{IPR}(L)\rangle_{\mathrm{Pixel}} = \frac{1}{N}\sum_{i=1}^{N}\int_0^L\int_0^L E_i^4(x,y)dxdy, \tag{3}$$

where E_i is the ith eigenfunction of the Hamiltonian in Eq. (2) of an optical lattice (i.e., an IPR pixel) of size $L\times L$; $N=L_a^2$ [$L_a=L/a$ (lattice size), $a=dx=dy$] is the total number of

a)Electronic mail: pradhan@northwestern.edu.

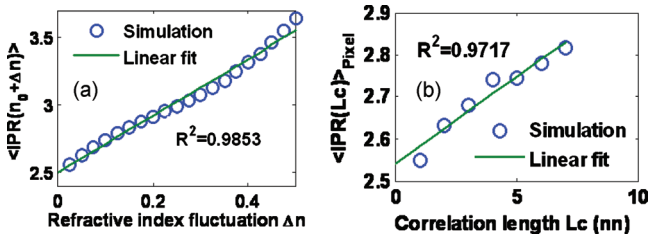

FIG. 1. (Color) Numerical simulation results: (a) IPR(Δn) vs Δn and (b) IPR(Lc) vs Lc plots.

the eigenfunctions; and $\langle\ \rangle_{\text{Pixel}}$ denotes the average over all of the N eigenfunctions of the IPR pixel.

Figure 1 shows the numerical simulation of $\langle \text{IPR}(\Delta n)\rangle$ versus Δn [Fig. 1(a)] and $\langle \text{IPR}(\Delta n)\rangle$ versus Lc (spatial correlation length) [Fig. 1(b)] of the IPR calculations by using the tight-binding model [i.e., using Eqs. (2) and (3) and $t=1$]. The results show that IPR linearly varies with Δn and Lc.

$$\langle \Delta\text{IPR}(\Delta n)\rangle_{\text{Pixel}} = \langle \Delta\text{IPR}(n_0+\Delta n)\rangle_{\text{Pixel}} - \langle \Delta\text{IPR}(n_0)\rangle_{\text{Pixel}} \cong 2\Delta n, \quad \text{and} \quad \langle \Delta\text{IPR}(Lc)\rangle_{\text{Pixel}} = \alpha Lc, \quad (4)$$

where α is a proportionality constant, which linearly depends on Δn.

To *validate* that the IPR technique can be used for biological systems, we prepared a model disordered media system using Fe_3O_4 dielectric nanoparticles according to the protocol described in Ref. 15. The nanoparticles in a hexane solution of different concentrations were spread over copper meshes present on formvar thin films. Then, the samples were ultrasonicated to avoid periodic lattice formation and to achieve a random distribution of the nanoparticles on the thin film. Finally, the nanoparticle solutions were dried on the films, and the disordered media consisting of thin film and nanoparticles were prepared. The mean diameter of the nanoparticles was 6 nm and the standard deviation was 2 nm. Sources of disorder in these 2D thin-film-nanoparticle systems resulted from (i) the mass-density fluctuations of the formvar thin film (with dried hexane masses), (ii) the spatial 2D random positions of the nanoparticles, and (iii) the size fluctuations of the nanoparticles [see Figs. 2(a)–2(d) and 2(q)].

TEM imaging. TEM micrographs were obtained (TEM) (JEM-1400, JEOL, Tokyo, Japan) for each of the prepared samples having varying concentrations of nanoparticles on the thin films. A 200 keV electron beam with a fixed magnification (40 000×) was used for the imaging.

Figures 2(a)–2(d) show the representative TEM grayscale images (micrographs) of relatively uniform background (pure formvar dielectric thin film) and three different concentrations of nanoparticles on the thin film (with deposited hexane). Figures 2(e)–2(h) show the corresponding IPR pixel images, and Figs. 2(i)–2(l) show the $\langle \text{IPR}\rangle_{\text{Pixel}}$ distributions, respectively. These results clearly show that IPR values increase with increasing concentration of nanoparticles (i.e., disorder strength).

Figure 2(m) shows that the length scale-dependent average of $\langle\langle \text{IPR}(L)\rangle_{\text{Pixel}}\rangle$ for each disorder sample increases with the sample (i.e., lattice) size and disorder concentration for the three different sample types. As shown in Fig. 2(n), the average increases with increased L, and then it saturates to a universal value of IPR ~ 2.5 at $L\times L=(308\ \text{nm})^2$ for the uniform sample [e.g., Fig. 2(a)]. The experiments with nanoparticles further confirm that the average IPR value increases with the increase of nanoparticle density N_p [Fig. 2(p)] and with the product of density fluctuations $\Delta n/n_0$ and short-range correlation length Lc, that is, $(\Delta n/n_0 Lc)$ [Fig. 2(o)], consistent with IPR theory. Figure 2(q) shows the *similarities* of $I_{\text{TEM}}(L)s$ for both nanoparticle model and biological cells. Overall, the validation study shown in Fig. 2 shows that

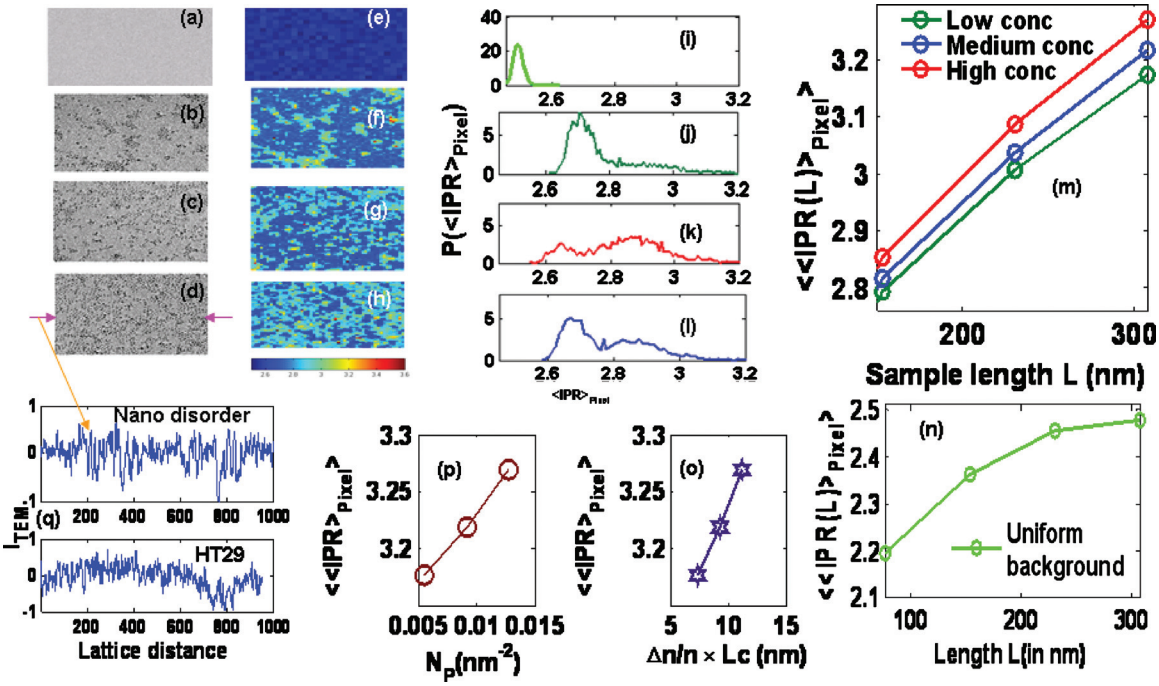

FIG. 2. (Color) [(a)–(d)] Representative grayscale images of uniform background of dielectric thin film and dielectric nanoparticles on dielectric thin films with increasing particle concentration (or disorder strength). [(e)–(h)] Corresponding IPR images. [(i)–(l)] Distribution $P(\langle \text{IPR}\rangle_{\text{Pixel}})$ plots. (m) $\langle \text{IPR}(L)\rangle_{\text{Pixel}}$ vs L plots for three different disordered samples, and (n) Same as (m) for uniform sample. (o) $\langle\langle \text{IPR}(\Delta n/n_0\times L_c)\rangle\rangle$ vs $(\Delta n/n_0\times Lc)$ plot and (p) $\langle\langle \text{IPR}(Np)\rangle\rangle$ vs Np plot. (q) $I_{\text{TEM}}(L)$ plots for nanodisordered sample (top) and the same for a HT29 cell [Fig. 3(a)] (bottom).

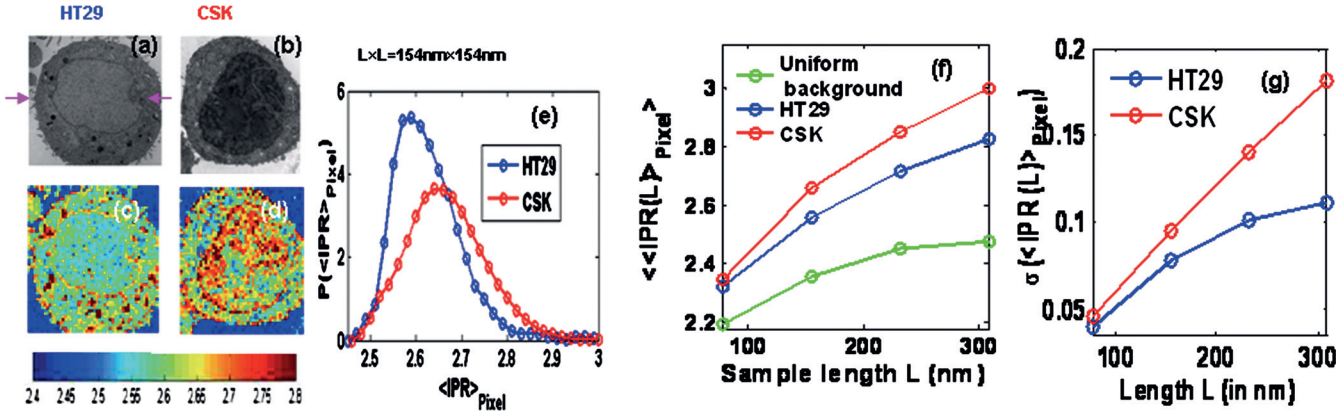

FIG. 3. (Color) [(a) and (b)] Representative TEM images of HT29 cells and CSK cells. [(c) and (d)] Corresponding $\langle \mathrm{IPR} \rangle_{\mathrm{Pixel}}$ image. (e) Relative $\langle \mathrm{IPR}(L) \rangle_{\mathrm{Pixel}}$ distributions for HT29 and CSK cells. (f) Ensemble averaged $\langle \langle \mathrm{IPR}(L) \rangle_{\mathrm{Pixel}} \rangle$ vs L plots for (i) uniform sample (or background), (ii) HT29 cells, and (iii) CSK cells. (g) Standard deviation $\sigma(\langle \mathrm{IPR}(L) \rangle_{\mathrm{Pixel}})$ vs L plots for HT29 cells and CSK cells. Because of the large number of samples (~50 000), the error bars are negligible.

nanoscale minute disorder can be quantified by the IPR technique, which can distinguish statistically significant differences between two disordered systems.[2,3]

To study the changes of *nanoscale mass-density fluctuations* with cancerous growth in heterogeneous biological cells, we used a well-studied colonic cancer cell line model, HT29 cells, and their genetic variance CSK constructs [constructed by a knockdown of tumor-suppressor C-terminus src kinase (CSK) gene], which are known to be more aggressive in cancerous growth. These two cell types are cytologically, i.e., microscopically, indistinguishable, but they have different neoplastic potential with corresponding nanoscale differences. The preparation of these cells is described elsewhere.[8] Both HT29 cells and their CSK construct cells underwent a standard sample preparation protocol for TEM imaging, including fixing, staining, embedding, sectioning and, finally, performing TEM imaging, as described earlier for the nanoparticles.[7]

Figures 3(a) and 3(b) show representative TEM gray-scale images of HT29 cells and CSK constructs. The corresponding IPR images are shown in Figs. 3(c) and 3(d) and relative $P(\langle \mathrm{IPR} \rangle_{\mathrm{Pixel}})s$ in Fig. 3(e). Using an analytical method similar to that described in Fig. 2 for nanoparticles, we plotted in Figs. 3(f) and 3(g) the length scale-dependent average and std, i.e., $\langle \langle \mathrm{IPR}(L) \rangle_{\mathrm{Pixel}} \rangle$ and $\sigma(\langle \mathrm{IPR}(L) \rangle_{\mathrm{Pixel}})$, which shows that these values are higher for CSK constructs relative to HT29 cells for all L. For example, $\langle \langle \mathrm{IPR}(L) \rangle_{\mathrm{Pixel}} \rangle$ values for the uniform background, HT29 cells, and CSK constructs are 2.5, 2.8259, and 2.9978, respectively [averaged over ~20 cells for each cell type and calculated over ~50 000 pixels (or samples) with student t-test, two-tailed p-value $< .05$], are statistically significantly different. The higher values of the average and the std for CSK cells correspond to the higher disorder strength by the larger nanoscale mass-density fluctuations.

In summary, we report an IPR imaging and analysis technique to quantify the light-localization (i.e., spatial localization of eigenfunctions) properties of nanoscale mass-density fluctuations of heterogeneous disordered systems via TEM imaging. We have validated the IPR technique using thin-film-nanoparticle systems. Then, we applied IPR analysis to show a higher degree of disorder at the nanoscale for CSK construct cells, with their more aggressive growth/proliferation, relative to HT29 control cells. Here, all the cells were cytologically indistinguishable. Thus, the results of the IPR study via TEM imaging show an increase of nanoscale disorder with increasing degree of carcinogenesis, consistent with our previous optical results reported in Refs. 8–10 and 16. Based on our fundamental physics concept, we anticipate that IPR analyses of TEM images will have potential applications for characterization of nanoscale mass-density fluctuations in nanostructures as well as cells and tissue in nanotechnology and biophysics research.

This work was supported by NIH grants (Grant Nos. R01EB003682, R01CA128641, and U54CA143869) and NSF Grant No. CBET-0937987. V.P.D. acknowledges support from NIH/NCI PS-OC Grant No. DMR-0603184 and NIH-CCNE (Northwestern) Grant No. U54CA119341. Parts of the experiments were done at the EPIC/NIFTI facility of the NU*ANCE* Centre (supported by NSF-NSEC, NSF-MRSEC, Keck Foundation, the State of Illinois, and Northwestern University) at Northwestern University. P.P. thanks S. Sridhar (Northeastern University, Boston) for many insightful discussions.

[1] B. Kramer and A. MacKinnon, Rep. Prog. Phys. **56**, 1469 (1993).
[2] Y. V. Fyodorov and A. D. Mirlin, Phys. Rev. B **55**, R16001 (1997).
[3] V. N. Prigodin and B. L. Altshular, Phys. Rev. Lett. **80**, 1944 (1998).
[4] P. Pradhan and S. Sridhar, Phys. Rev. Lett. **85**, 2360 (2000).
[5] P. Pradhan and S. Sridhar, Pramana, J. Phys. **58**, 333 (2002).
[6] T. Schwartz, G. Bartal, S. Fishman, and M. Segev, Nature (London) **446**, 52 (2007).
[7] J. J. Bozzola and L. Dee, *Electron Microscopy: Principles and Techniques for Biologists* (Jones and Bartlett, Boston, 1999).
[8] H. Subramanian, P. Pradhan, Y. Liu, I. R. Capoglu, X. Li, J. D. Rogers, A. Heifetz, D. Kunte, H. K. Roy, A. Taflove, and V. Backman, Proc. Natl. Acad. Sci. U.S.A. **105**, 20118 (2008).
[9] H. Subramanian, P. Pradhan, Y. Liu, I. R. Capoglu, J. D. Rogers, H. K. Roy, R. E. Brand, and V. Backman, Opt. Lett. **34**, 518 (2009).
[10] H. Subramanian, H. K. Roy, P. Pradhan, M. J. Goldberg, J. Muldoon, R. E. Brand, C. Sturgis, T. Hensing, D. Ray, A. Bogojevic, J. Mohammed, J. S. Chang, and V. Backman, Cancer Res. **69**, 5357 (2009).
[11] R. Barer, K. F. A. Ross, and S. Tkaczyk, Nature (London) **171**, 720 (1953).
[12] E. Zeitler and G. F. Bahr, J. Appl. Phys. **33**, 847 (1962).
[13] M. Loferer-Krossbacher, J. Klima, and R. Psenner, Appl. Environ. Microbiol. **64**, 688 (1998).
[14] J. M. Schmitt and G. Kumar, Opt. Lett. **21**, 1310 (1996).
[15] S. Sun, Hao Zeng, D. B. Robinson, S. Raoux, P. M. Rice, Shan X. Wang, and G. Li, J. Am. Chem. Soc. **126**, 273 (2004).
[16] D. Damania, H. Subramanian, A. Tiwari, Y. Stypula, D. Kunte, P. Pradhan, H. Roy, and V. Backman, Biophys. J. **99**, 989 (2010).